J. Fluid Mech. (1992), *vol.* 243, *pp.* 247–259
Printed in Great Britain

Laboratory studies on the surface drift current induced by wind and swell

By ZHAN CHENG[1] AND HISASHI MITSUYASU[2]

[1] National Research Center for Marine Environment Forecasts, no. 8 Da Hui Si, Hai Dian District, Beijing, China

[2] Research Institute for Applied Mechanics, Kyushu University 87, Kasuga, 816 Japan

(Received 2 April 1991 and in revised form 17 March 1992)

Systematic measurements of the surface drift current, the wind profile over the water surface and the wave spectra have been made for (i) pure wind-waves, (ii) a co-existing system of wind-waves and swell propagating against the wind, and (iii) a co-existing system of wind-waves and swell propagating in the direction of the wind. The surface drift current is gradually intensified by the swell propagating against the wind when the swell steepness increases. The maximum increase of the surface drift velocity caused by the opposing swell is about 46% of the surface drift velocity for pure wind-waves at the same wind speed. Such a phenomenon was not observed when the swell was propagating in the direction of the wind.

1. Introduction

The formation of surface drift current in the ocean is of great interest both in oceanography and in ocean engineering. During the last forty years, there have been several laboratory studies of wind-induced drift currents (Keulegan 1951; Shemdin 1972; Wu 1973; Phillips & Banner 1974; Wu 1975). Wu (1975) shows that the ratio of the surface drift velocity to the wind friction velocity as a whole has no systematic dependence upon the wind friction velocity. However, the previous works are confined to the case of pure wind-waves. In many cases in the ocean, the wind-waves generated by a local wind co-exist with swells which are generated in the other areas and not necessarily propagating in the direction of the local wind. As far as we know, however, there have been no experimental studies of the effect of swell on the wind-induced drift currents except for the theoretical study of Phillips & Banner (1974).

The experiment was carried out to clarify the effect of swell on the wind-induced drift current. Systematic measurements of the surface drift current, waves and wind profiles over the water surface were made for: (i) pure wind-waves, (ii) a co-existing system of wind-waves and swell propagating against the wind and (iii) a co-existing system of wind-waves and swell propagating in the direction of the wind. The present results for pure wind-waves are compared with those of Wu (1973). The most interesting finding of the present study is that the surface drift current is intensified by the existence of opposing swell when the swell steepness increases. However, such a phenomenon was not observed in the experiment where the swell is propagating in the direction of the wind.

2. Equipment and procedures

2.1. *The wind-wave flume and the measurements*

The experiment was carried out in a wind-wave flume 0.8 m high, 0.6 m wide, and with a usual test section 15 m long. In experiment 1, where swell is propagating against the wind, water depth was kept at 0.353 m. In experiment 2, where swell is propagating in the direction of the wind, water depth was kept at 0.333 m. The water depth was decreased for experiment 2 because when swell is propagating in the direction of the wind, the growth of the swell is expected and the crest of the swell may touch the transition plate in the tank. The arrangement of the equipment for experiment 1 is shown schematically in figure 1. A beach for absorbing swell energy, a centrifugal fan for blowing wind through the flume and a transition plate for thickening the air boundary layer were situated on the upwind side of the test section (the fan not shown in figure 1). At the downwind side, a filter made of vinylon net was installed across the water section for absorbing the downwind-propagating wind waves. A flap-type wave generator at the downwind side was used for generating swell (regular oscillatory waves). The arrangement for experiment 2 is almost the same to that for the experiment 1 except that the wind direction is opposite (from right to left). The connection of the fan with the flume was changed to suck the air, and the air was carried on to the water surface at the outlet in figure 1 by setting an elbow that contained turning vanes, honeycombs, a screen and a transition plate. The detail of the arrangement can be found in Mitsuyasu & Honda (1982), though the figure is turned 180°.

Wind speed U_r in the flume was changed stepwise as $U_r = 3$, 5 and 7 (m/s), and monitored with a Pitot tube installed above the transition plate. Here, the wind speed U_r corresponds roughly to a cross-sectional mean speed after the correction of a small change in the cross-sectional area of the tank. Vertical wind profiles over the water surface were measured with another Pitot tube at the fetch $F = 8$ m, where F was measured from the tip of the transition plate (figure 1). For experiment 2 the fetch is shorter than that for experiment 1. If we consider the elbow and the transition plate which are not shown but actually installed at the wind outlet in figure 1, the fetch in experiment 2 is approximately 3.5 m. Accurate measurements of the drift current were difficult in high-speed wind owing to the scatter of the paper float. That is the reason why the maximum wind speed is limited to 7 m/s.

The period of the swell in the tank was kept at $T = 1.024$ s, and the steepness of the swell without wind action was changed stepwise as $H_0/L = 0.01$, 0.02, 0.03 and 0.04. The waves were measured simultaneously at three stations, $F = 6$, 8 and 10 (m) with capacitance-type wave gauges (figure 1). The reasons for the choice of the wave period $T = 1.024$ s are as follows. First, the change of the swell of this period is very small along the fetch even under the wind action, that makes the phenomena simpler. Secondly, when we digitize the wave record with a sampling frequency 200 Hz, 2^n data which are used for FFT analysis give an integral multiple number of the regular waves. The latter reduces the leakage effect in the spectral analysis.

The surface drift velocity was determined by measuring the time required for thin waxed-paper floats ($\phi = 5$ mm) to travel a distance of 4 m centred at $F = 8$ m in the flume. The lapse time was recorded on Seiko-129 type digital stopwatch. The measurements were repeated 20 times and the averaged value of the drift velocity was used for the analysis.

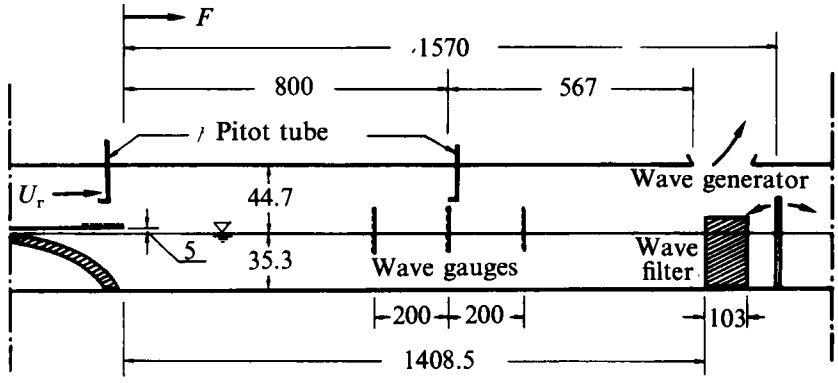

FIGURE 1. Schematic diagram of experimental arrangements for experiment 1 (units in cm).

2.2. *Experimental procedure*

Calibrations of the rotation (r.p.m.) of the wind blower versus the reference wind speed U_r and the stroke of the wave generator versus the wave height were done before the experiment. After the calibrations, experimental conditions, such as the reference wind speed and the period and height of the regular water waves could be controlled by a microcomputer.

In each experiment, the wind blower was started immediately after the start of the wave generator and the measurement of the wind profile over the wave surface was made 5 min after the start of the wind blower, when the wave system had reached a stationary state. It took about an hour for the measurement of the wind profile, and then the measurement of the surface drift current was begun. The measurements were arranged in this way because the time needed for the drift current to reach a stationary state is much longer than those required for the wind and wind-waves.

The waves were measured independently after the measurements of the wind profile and the surface drift velocity, because the wave gauges disturb the wind and current fields.

3. Analysis of the wave data

The wave records of each run were digitized at the sampling frequency of 200 Hz. From the wave records of 11 min for each run we obtained 32 samples of the wave data, each of which contained 4096 data points. Power spectra of waves were computed through a fast-Fourier-transform procedure for each sample of the wave data. The sample of the 32 spectra was used for further analysis. Owing to the procedure described in §2, the leakage effect of the spectral components of the regular waves was negligibly small. The frequency resolution of the wave spectra was $\Delta f = 4.88 \times 10^{-2}$ Hz.

4. Results

4.1. *Wind profile over the water surface*

Vertical wind profiles $U(z)$ over the water surface were measured for the co-existing system of wind-waves and swell propagating against the wind and for the co-existing system of wind-waves and swell propagating in the direction of the wind. Some

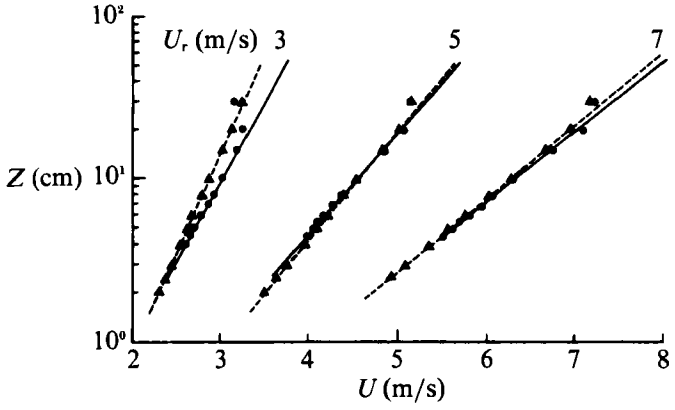

FIGURE 2. Wind profiles over the water surface for pure wind waves and the co-existing system of wind-waves and the swell propagating against the wind. H_0/L: ▲, 0 (pure wind-waves); ●, 0.04.

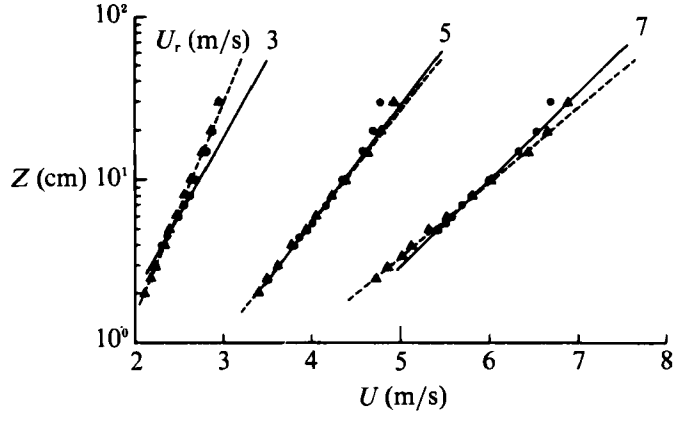

FIGURE 3. Wind profiles over the water surface for pure wind-waves and the co-existing system of wind-waves and the swell propagating in the direction of the wind. H_0/L: ▲, 0 (pure wind-waves); ●, 0.04.

examples of the wind profiles are shown in figure 2 (experiment 1) and figure 3 (experiment 2). All profiles show logarithmic distributions,

$$U(z) = \frac{U_*}{\kappa} \ln \frac{Z}{Z_0}, \tag{1}$$

where $U_* = (\tau_s/\rho_a)^{\frac{1}{2}}$ (τ_s is the wind shear stress, ρ_a is the density of the air) is the friction velocity of the wind, κ is Kármán's constant (≈ 0.40), and Z_0 is a roughness parameter of the water surface. The values of U_* and Z_0 were determined from the wind profile $U(z)$ near the water surface by applying the logarithmic distribution (1). The friction velocity U_* thus determined is used for the analysis of the surface drift velocity.

4.2. *The drag coefficient of the water surface*

The wind speed U_{10} at the height $Z = 10$ m, was determined from the data of U_* and Z_0 by extrapolating the logarithmic wind profile (1). By using a definition of the drag coefficient C_D,

$$C_D = \tau_s/\rho_a U_{10}^2 = (U_*/U_{10})^2, \tag{2}$$

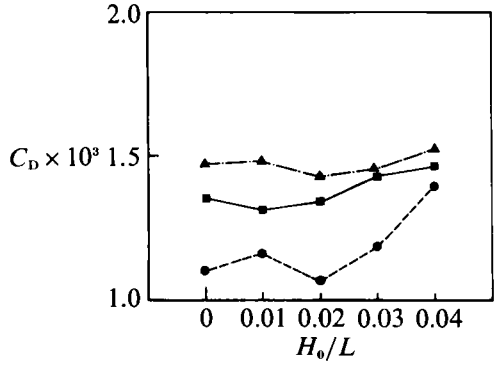

FIGURE 4. The drag coefficient $C_D = (u_*/U_{10})^2$ versus the swell steepness H_0/L for the co-existing system of wind-waves and the swell propagating against the wind. U_r(m/s): ●, 3; ■, 5; ▲, 7.

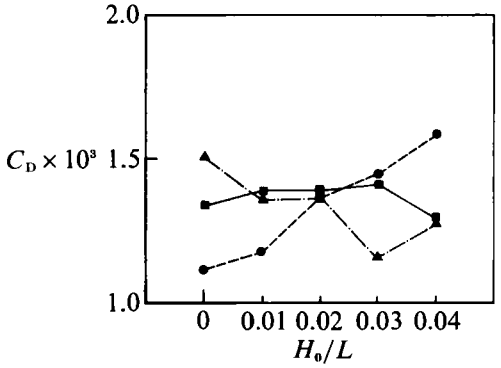

FIGURE 5. The drag coefficient $C_D(\equiv (u_*/U_{10})^2)$ versus the swell steepness H_0/L for the co-existing system of wind-waves and the swell propagating in the direction of the wind. U_r(m/s): ●, 3; ■, 5; ▲, 7.

C_D can be calculated from the measured values of U_* and U_{10}. Figure 4 shows the relation between the drag coefficient C_D and the steepness H_0/L of the swell propagating against a wind for three different wind speeds, $U_r = 3$, 5, 7 m/s. It can be seen from figure 4 that the drag coefficient of the water surface increases clearly with the wind speed U_r but it is not much affected by the swell steepness, except for the case of the lowest wind speed $U_r = 3$ m/s. For the wind speed $U_r = 3$ m/s, the drag coefficient C_D increases clearly with the increase of the swell steepness, though the reason for this is not clear now.

When swell is propagating in the direction of the wind, the effect of the swell on the drag coefficient of the water surface is very complicated (as shown in figure 5). The drag coefficient C_D increases clearly with the swell steepness for the wind speed $U_r = 3$ m/s as in the case of the swell propagating against the wind, C_D is not much affected by the swell steepnes for the wind speed $U_r = 5$ m/s, but C_D decreases with the increase of swell steepness for the wind speed $U_r = 7$ m/s. That is, the effect of swell steepness on the drag coefficient is different depending on the wind speed when the swell is propagating in the direction of the wind. However, more detailed discussions on C_D are left for future studies, because the present data is not sufficient for more detailed analysis and our main purpose of the present study is the drift current.

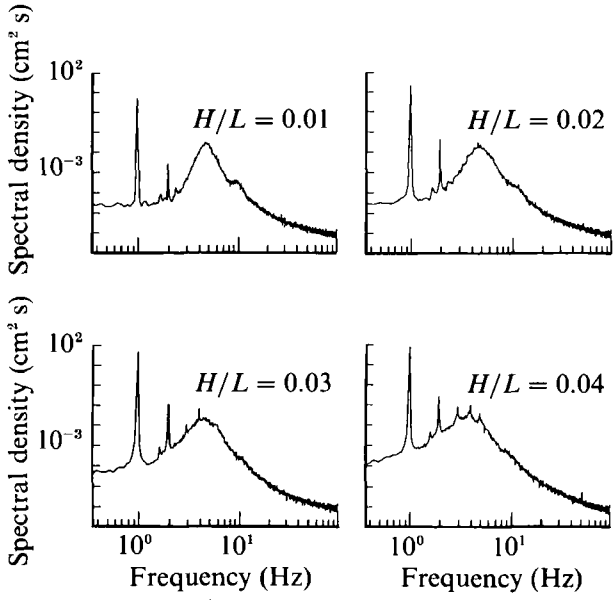

FIGURE 6. Power spectra of the co-existing systems of wind-waves and the swell propagating against the wind. $U_r = 5$ m/s and $F = 8$ m. Swell steepness H_0/L: 0.01, 0.02, 0.03 and 0.04.

4.3. *Wave properties*

The measurement of waves was done mainly to monitor the change of an opposing swell under the action of the wind and the change of wind waves by a co-existing swell. Some examples of the spectra of co-existing systems of wind-waves and an opposing swell are shown in figure 6, where the wind speed is $U_r = 5$ m/s and the fetch is $F = 8$ m. In order to separate the total wave energy into the energy of the swell E_s and that of wind waves E_w, we first eliminated the fundamental spectral peak of the swell and the spectral peaks corresponding to the higher harmonics of the swell by eliminating nine spectral points at or near each spectral peak and applying a linear interpolation to each spectral gap of the eliminated spectral points. In this way we obtained the spectrum of wind waves co-existing with swell. Then we determined the energy E_w of the wind-waves by integrating the wind-wave spectrum. The energy E_s of the swell is obtained by subtracting the wind-wave energy E_w from the total wave energy E_t of the co-existing system as

$$E_s = E_t - E_w. \tag{3}$$

The present method for separating the energy of wind-waves and that of the swell is different to that used by Mitsuyasu & Yoshida (1991). This is because at low wind speed, spectral peaks corresponding to the higher harmonic of the swell, which appear in the frequency region of the wind-wave spectrum, contribute a significant fraction to the spectrum of the co-existing system. From the value of E_s determined above we calculated, approximately, the wave height H of the swell under the action of the wind by using an ordinary relation, $H = 8(E_s)^{\frac{1}{2}}$.

As previously mentioned, a relatively long regular water-wave ($T = 1.024$ s and $L \approx 1.5$ m) was used in the experiment in order to reduce the change in the wave height of the swell propagating under the action of the wind. In fact, relative changes in the wave height of the swell owing to the wind action were

$$(H - H_0)/H_0 < 5\%, \tag{4}$$

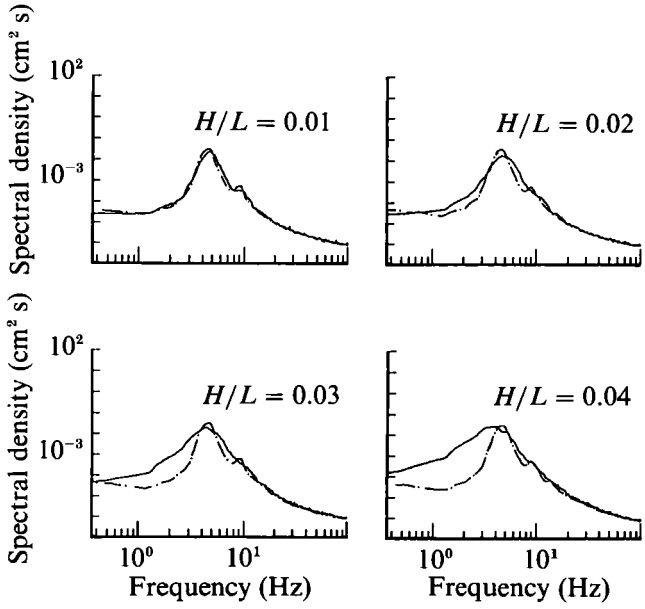

FIGURE 7. Power spectra of the pure wind-waves and wind-waves affected by the opposing swell. $U_r = 5$ m/s and $F = 8$ m. -·-·-, the pure wind-waves; ——, wind-waves affected by the opposing swell. Swell steepness H_0/L: 0.01, 0.02, 0.03 and 0.04.

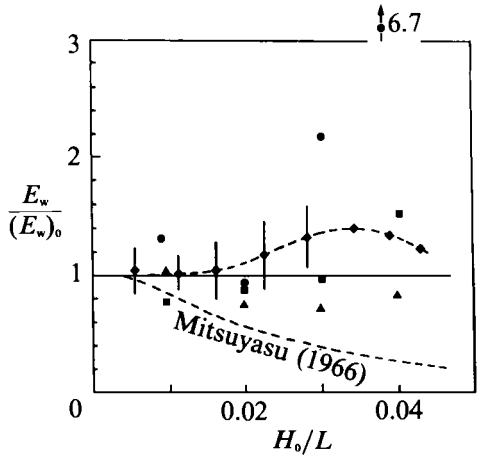

FIGURE 8. The normalized wind-wave energy $E_w/(E_w)_0$ versus the steepness H_0/L of the opposing swell. U_r(m/s): ●, 3; ■, 5; ▲, 7; ◆, ◆, the data of Mitsuyasu & Yoshida (1991). The data for $U_r = 3$ m/s and $H_0/L = 0.04$ is $E_w/(E_w)_0 = 6.7$ and out of the figure.

for all experiments except for the case of $U_r = 7$ m/s and $H_0/L = 0.01$, for which the relative change is about 25%. In (4) H is the wave height of the swell under the action of the wind and H_0 is the wave height of the swell without wind action. Therefore, the original wave steepness H_0/L is used tentatively as a parameter representing the swell steepness.

Figure 7 shows the wind-wave spectra of the co-existing systems of the wind-waves and the opposing swell, where the spectrum of the swell is eliminated by the method mentioned previously. In this figure, an 11-points triangular filter is used to smooth further the high-frequency part of the wind-wave spectrum. All spectra shown in

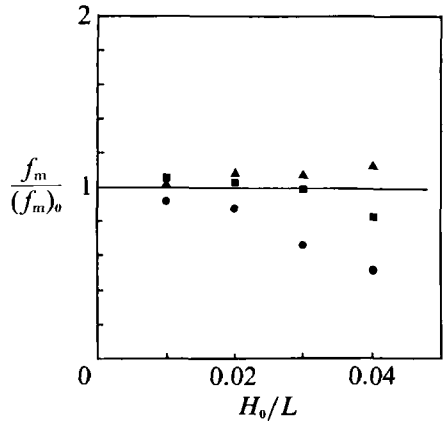

FIGURE 9. The normalized spectral peak frequency $f_m/(f_m)_0$ of the wind-wave spectra versus the swell steepness H_0/L. U_r(m/s): ●, 3; ■, 5; ▲, 7.

figure 7 are for wind speed $U_r = 5$ m/s and fetch $F = 8$ m, while the swell steepness changes stepwise from 0.01 to 0.04. The spectrum of the pure wind-waves at the same wind speed and the same fetch is superimposed in each figure for comparison. When the swell exists, the energy of the spectral peak of wind-waves decreases, but the energy of the spectrum in the other regions around the spectral peak increases. The increase of the spectral energy in a low-frequency region $f < f_m$ is especially remarkable for the cases of the swell steepness $H_0/L = 0.03$ and 0.04. In other words, the spectrum of wind-waves becomes a little wider by the existence of the opposing swell. This phenomenon is also observed in the cases of the wind speeds $U_r = 3$ and 7 m/s. Another feature demonstrated in figure 7 is that the high-frequency portions of the wind-wave spectrum ($f > 10$ Hz) are not much affected by the opposing swell.

The normalized wind-wave energy $E_w/(E_w)_0$ and the normalized spectral peak frequency $f_m/(f_m)_0$ for wind-waves co-existing with the opposing swell are shown in figures 8 and 9, respectively, as a function of the swell steepness. Here $(E_w)_0$ and $(f_m)_0$ denote the energy and the spectral peak frequency for the pure wind-waves at the same wind speed and the same fetch. These figures show that both the wave energy and the spectral peak frequency of the wind-waves are not much changed by the increase of the opposing swell steepness except for the case of low wind speed $U_r = 3$ m/s, where wind-wave energy E_w increases and the spectral peak frequency f_m decreases considerably with the increase of the swell steepness. It is interesting to find that the change of the normalized wind-wave energy by the steepness of the opposing swell is similar to the change of the drag coefficient shown in figure 4. This fact suggests that the change of the wind-wave energy by the opposing swell is due to the change of the wind shear stress, which was caused by the opposing swell.

Quite recently, Mitsuyasu & Yoshida (1991) carried out a laboratory experiment on the growth of wind-waves co-existing with an opposing swell, in which the wind speed extended to a higher speed range. Although the results scatter considerably, their results show that the growth of the wind-waves is not much affected by the swell when the swell steepness is relatively small but it is intensified by the swell when the swell steepness increases. The previous results are superimposed in figure 8.

These properties of wind-waves co-existing with opposing swell are quite different from those of wind-waves co-existing with swell propagating in the direction of the wind. In the latter case (as previously shown by Mitsuyasu 1966 and Phillips &

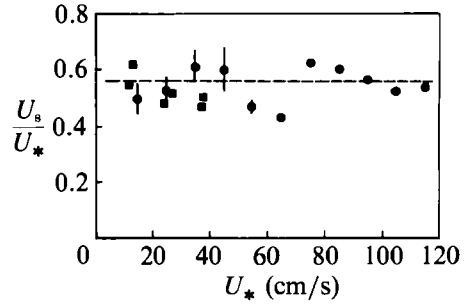

FIGURE 10. The dimensionless surface drift velocity U_s/U_* versus the wind friction velocity U_* for the pure wind-waves. ⧫, ●, Wu (1973); ■, the present data; ---, $U_s/U_* = 0.55$.

Banner 1974), the wind-waves attenuate considerably with the increase of the swell steepness as shown in the lower part of figure 8. Phillips & Banner (1974) proposed an attenuation mechanism of the wind-waves in the presence of wind drift and swell. Therefore, the effect of the swell on the growth of wind-waves is very different depending on the propagation direction of the swell. This phenomenon will be discussed separately in the near future.

4.4. *Surface drift velocity*

In each experiment, the measurement of the surface drift velocity was repeated 20 times. The mean value of the 20 samples was used to calculate the magnitude of the surface drift velocity. The ratio of the standard deviation of the 20 samples to the average value is less than 10% for all measurements.

4.4.1. *Results for pure wind-waves*

As pointed out by Wu (1973), since the drift current is mainly generated by the wind shear stress, the wind friction velocity is the most important parameter for determining the surface drift velocity. The dependence of the dimensionless surface drift velocity U_s/U_* on the wind friction velocity U_* is shown in figure 10. The measured data of Wu (1973) are also shown in the same figure for comparison. In general, the present data of U_s/U_* for pure wind-waves are consistent with those of Wu (1973), and both sets of data show that U_s/U_* is roughly independent of the wind friction velocity U_*. The average value of U_s/U_* for the data of Wu (1973) is

$$U_s/U_* = 0.55. \tag{5}$$

For our present data, the average value of U_s/U_* for the case of pure wind-waves is

$$U_s/U_* = 0.52. \tag{6}$$

It should be noted, however, that if we look at the data closely the value of U_s/U_* for our present data slightly decreases with the increase of U_*, though the range of U_* is limited.

4.4.2. *Results for the co-existing system of wind-waves and the swell propagating against the wind* (*experiment* 1)

Figure 11 shows the effect of the swell on the surface drift current where the swell is propagating in the opposite direction to the wind. In order to compare the results with those in figure 10 for the case of pure wind-waves, the dimensionless drift velocity U_s/U_* is plotted against U_*. The results of figure 11 show clearly that U_s/U_*

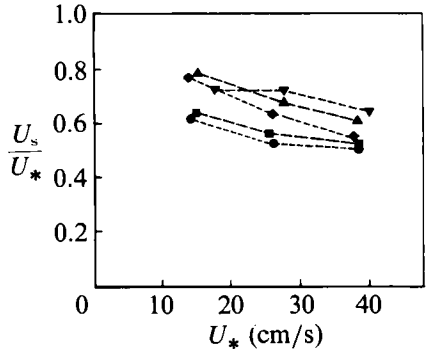

FIGURE 11. The dimensionless surface drift velocity U_s/U_* versus the wind friction velocity U_* for the co-existing system of wind-waves and the swell propagating against the wind. H_0/L: ●, 0.00; ■, 0.01; ◆, 0.02; ▲, 0.03; ▼, 0.04.

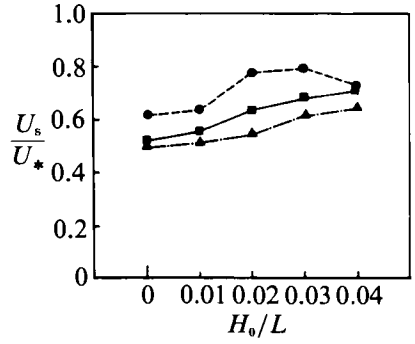

FIGURE 12. The dimensionless surface drift velocity U_s/U_* versus the swell steepness H_0/L for the co-existing system of wind-waves and the swell propagating against the wind. U_r(m/s): ●, 3; ■, 5; ▲, 7.

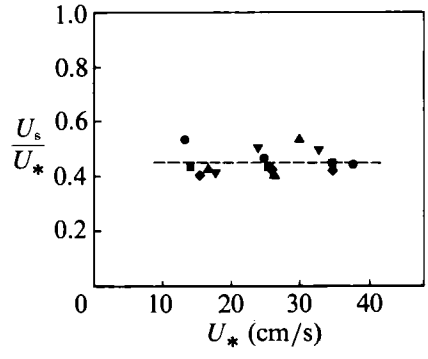

FIGURE 13. The dimensionless surface drift velocity U_s/U_* versus the wind friction velocity U_* for the co-existing system of wind-waves and the swell propagating in the direction of the wind. H_0/L: ●, 0.00; ■, 0.01; ◆, 0.02; ▲, 0.03; ▼, 0.04; the dashed line is $U_s/U_* = 0.46$.

decreases with the increase of U_* as mentioned previously for the case of pure wind-waves, but U_s/U_* increases with the increase of the swell steepness H_0/L. Figure 12 is a different expression of the result shown in figure 11. Here U_s/U_* is plotted against the swell steepness H_0/L by taking the reference wind speed U_r as a parameter. According to the results shown in figure 12, U_s/U_* increases with the increase of the

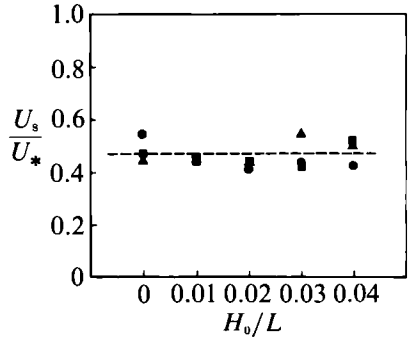

FIGURE 14. The dimensionless surface drift velocity U_s/U_* versus the swell steepness H_0/L for the co-existing system of wind-waves and the swell propagating in the direction of the wind. U_r(m/s): ●, 3; ■, 5; ▲, 7; ---, $U_s/U_* = 0.46$.

swell steepness, but it tends to saturate for very large swell steepness. It should be noted that the increase of the surface drift current by the co-existing swell is not due to the Stokes drift of the swell, because the Stokes drift of the swell in this case is in the opposite direction to that of the wind-induced surface drift. We also measured the Stokes drift of the swell without wind action, which was found to be negligibly small as compared to the pure wind drift in our experiment, even for the largest swell steepness $H_0/L = 0.04$.

4.4.3. *Results for the co-existing system of wind-waves and the swell propagating in the direction of the wind* (*experiment* 2)

The change of the surface drift current caused by the swell propagating in the direction of the wind is shown in figures 13 and 14. These figures show that when the swell is propagating in the direction of the wind the effect of the swell on the surface drift current is very small and the data scatter around

$$U_s/U_* = 0.46. \tag{7}$$

The value of $U_s/U_* = 0.46$ for this case is a little smaller than $U_s/U_* = 0.52$ for the pure wind waves in experiment 1. The small difference of U_s/U_* may not be attributed to the effect of the swell, because the values of U_s/U_* for pure wind waves in the present case are not very different to the values of U_s/U_* for the co-existing system as shown in figures 13 and 14. The small difference in the values of U_s/U_* for the pure wind waves in experiment 1 and experiment 2, may be attributed to the difference in the boundary condition of the experiment. In experiment 1, the wind is blowing from left to right in the wind-wave tank shown in figure 1, while in experiment 2 the wind is blowing from right to left and the fetch is much shorter than that in experiment 1.

4. Discussion

Phillips & Banner (1974) presented a theoretical model for the change of wind drift caused by the swell in relation to the wave breaking in the presence of the surface current. According to their theory, swell changes the surface drift induced by the wind. When the swell propagates in the direction of the wind, the distribution of the surface drift velocity q with respect to the phase of the swell is

$$q = (C-u)-[(C-u)^2-q_0(2C-q_0)]^{\frac{1}{2}}, \tag{8}$$

where C and u are the phase speed and the horizontal component of the orbital velocity of the swell, respectively, and $q = q_0$ for $u = 0$. So q_0 can be considered as the surface drift velocity when there is no swell. The above equation can be rewritten as

$$\frac{q}{q_0} = \left(\frac{C}{q_0} - \frac{u}{q_0}\right) - \left[\left(\frac{C}{q_0} - \frac{u}{q_0}\right)^2 - \left(\frac{2C}{q_0} - 1\right)\right]^{\frac{1}{2}}. \tag{9}$$

In our present experiment, the horizontal component of the orbital velocity of the swell at the water surface can be approximated by

$$u = u_0 \cos\theta = \tfrac{1}{2} H\omega(\cosh kd/\sinh kd)\cos\theta, \tag{10}$$

where ω is the angular frequency of the swell, k the wavenumber of the swell, d the water depth and $\theta = kx - \omega t$. Substituting the experimental data $k = 4.30\ \mathrm{m}^{-1}$, $d = 0.333$ m and $\omega = 2\pi/T = 2\pi C/L$ into the above equation, we obtain

$$u = u_0 \cos\theta = 1.12\pi(H/L)\, C \cos\theta. \tag{11}$$

From the results of Phillips & Banner, the larger the values of u_0/C and q_0/C are, the larger the effect of swell on the wind-induced surface drift is. For the limiting case of our present experiment $U_r = 7$ m/s and $H_0/L = 0.04$, the values of u_0/C and q_0/C are, respectively,

$$u_0/C = 0.141, \quad q_0/C = 0.119. \tag{12}$$

For these values, the maximum surface drift calculated from (9), which occurs at the crest of the swell, is $q_{\max}/q_0 = 1.198$ and the minimum surface drift, which occur at the trough of the swell, is $q_{\min}/q_0 = 0.862$. On average, the change of the surface drift is $\bar{q}/q_0 \approx 1.03$. Therefore, even at the limiting case in our experiment, the average surface drift is little affected by the swell propagating in the direction of the wind. Comparing this result with the present data in figure 14, where the swell is propagating in the direction of the wind, we conclude that the present experimental result does not contradict with the theory of Phillips & Banner (1974).

When the swell is propagating against the wind, the distribution of wind-induced surface drift with respect to the phase of the swell is given by

$$q = -(C-u) + [(C-u)^2 + q_0(2C+q_0)]^{\frac{1}{2}}. \tag{13}$$

Thus

$$\frac{q}{q_0} = -\left(\frac{C}{q_0} - \frac{u}{q_0}\right) + \left[\left(\frac{C}{q_0} - \frac{u}{q_0}\right)^2 + \left(\frac{2C}{q_0} + 1\right)\right]^{\frac{1}{2}}. \tag{14}$$

For the limiting case of our experiment $U_r = 7$ m/s and $H_0/L = 0.04$, the values of u_0/C and q_0/C are, respectively,

$$u_0/C = 0.143, \quad q_0/C = 0.134. \tag{15}$$

In this case, the maximum surface drift calculated from (14), which also occurs at the crest of the swell, is $q_{\max}/q_0 = 1.144$ and the minimum surface drift, which occurs at the trough of the swell, is $q_{\min}/q_0 = 0.888$. On average, the change of the surface drift is $\bar{q}/q_0 \simeq 1.02$. That is, the average surface drift is little affected by the opposing swell, even at the limiting case in our experiment. Therefore, the large increase of the wind-induced drift current by the opposing swell, which is shown in figures 11 and 12, cannot be explained by the theoretical model of Phillips & Banner (1974).

Furthermore, according to the theoretical model of Phillips & Banner (1974), wind-waves should attenuate by breaking, owing to the enhanced surface drift current actually observed. However, the present results do not show the attenuation

of wind-waves by the opposed swell. On the contrary, the present result for the low-speed wind and the recent results by Mitsuyasu & Yoshida (1991) show the growth of wind-waves with an opposed swell when the swell steepness is relatively large. These facts show that we need to explore a new dynamical model, different from Phillips & Banner's, to describe the co-existing system of wind-waves and opposing swell. More detailed work will be done on this in the near future.

5. Conclusion

The most interesting finding of the present study is that the wind drift current is intensified by the swell propagating against the wind, and the surface drift velocity increases with the swell steepness. This kind of phenomenon is not observed when the swell is propagating in the direction of the wind.

In addition to the wind drift current, the growth of wind-waves also shows different changes depending on the direction of the swell. When the swell is propagating against the wind, wind-waves do not attenuate, while they attenuate when the swell is propagating in the direction of the wind.

When the swell is propagating in the direction of the wind, the changes of the wind drift current and the growth of wind-waves can be explained fairly well by the dynamical model proposed by Phillips & Banner (1974). However, when the swell is propagating against the wind, the changes cannot be explained by the proposed model. Further studies are needed to clarify the latter phenomena.

The authors wish to express their gratitude to Mr K. Marubayashi and Mr M. Ishibashi for their assistance in the laboratory experiment.

The study was conducted when Z.C. spent one year in the Research Institute for Applied Mechanics of Kyushu University supported by a fellowship from the Japan Society for the Promotion of Science.

REFERENCES

KEULEGAN, G. H. 1951 Wind tides in small closed channels. *J. Res. Natl Bur. Stand.* **46**, 358–381.

MITSUYASU, H. 1966 Interactions between water waves and winds (1). *Rep. Res. Inst. Appl. Mech., Kyushu University*, Vol. 14, No. 48, pp. 67–89.

MITSUYASU, H. & HONDA, T. 1982 Wind-induced growth of water waves. *J. Fluid Mech.* **123**, 425–442.

MITSUYASU, H. & YOSHIDA, Y. 1991 The effect of swell on the growth of wind waves. In *Oceanography of Asian Marginal Seas* (ed. K. Takano), pp. 381–391. Elsevier.

PHILLIPS, O. M. & BANNER, M. L. 1974 Wave breaking in the presence of wind drift and swell. *J. Fluid Mech.* **66**, 625–640.

SHEMDIN, O. H. 1972 Wind-generated current and phase speed of wind waves. *J. Phys. Oceanogr.* **2**, 411–419.

WU, J. 1973 Prediction of near-surface drift currents from wind velocity. *J. Hydraul. Div. ASCE* **99**, 1291–1302.

WU, J. 1975 Wind-induced drift currents. *J. Fluid Mech.* **68**, 49–70.